# Material characterisation for reliable and efficient springback prediction in sheet metal forming

**Andriy Krasowsky, Winfried Schmitt and Hermann Riedel**

Fraunhofer Institute for Mechanics of Materials, Woehlerstr. 11, D-79108 Freiburg, Germany

**Abstract**

In this paper, a novel experimental-numerical methodology for an accurate prediction of springback after sheet forming is presented. An advanced phenomenological material model is implemented in the FE-code ABAQUS. It includes the Bauschinger effect, the apparent reduction of the elasticity modulus at load reversal after plastic deformation, the strain rate dependency and the elastic-plastic anisotropy and its evolution during the forming process. The required material parameters are determined from stress-strain curves measured in tension-compression tests. These tests are carried out with a special test rig designed to avoid buckling of the specimen during compression. The benefits of this procedure for springback prediction are demonstrated. Additionally, parameters for the phenomenological models are determined from texture simulations.

**Keywords**: springback; tension-compression tests; Bauschinger effect; anisotropy; yield surface; texture

## Introduction

In sheet metal forming the elastic springback after the forming operation has always been a problem since it impairs the fitting accuracy, which is an important quality feature, for example in car bodies. In many cases the problem can be solved by the expertise of the toolmaker and of the press operator, possibly by modifying the tool surface in a few trial and error loops and by adjusting process parameters such as blankholder force.

However, the problem is aggravated for high-strength materials by the fact that the amount of springback generally increases with the yield stress (or, more precisely, with the ratio of yield stress to elasticity modulus), and is therefore more difficult to control. A lack of methods to predict springback for new high-strength steels may thus become a serious obstacle for their commercialisation.

In spite of many current research activities on the numerical prediction and compensation of springback, the situation is not satisfactory [1]. Unlike in other forming processes, the amount of springback in sheet metal forming depends on many physical factors, and its simulation is sensitive to numerical details. One of the most important aspects is the accurate description of the material behaviour under cyclic plastic loading. This is illustrated by considering the draw bending test shown in Figure 1. A blank strip clamped between die and blank holder is formed by the punch into a U-shaped profile (hat profile).

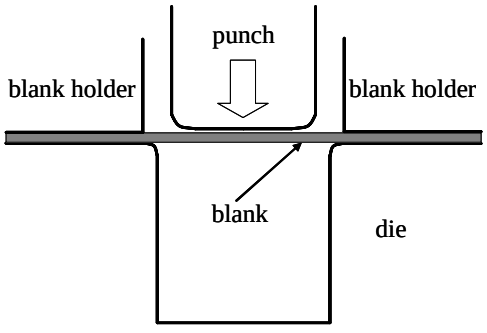


**Figure 1.** Draw bending test (schematic).

In Figure 2 the cause for springback is explained by considering the evolution of stresses when the sheet is drawn over the draw radius, for example of a hat profile. When entering the draw radius tensile stresses develop in the outer layer of the sheet and compressive in the inner layer (Figure 2, left). The subsequent straightening of the sheet inverts the stress distribution. Upon removal from the tool this residual stress will try to relax, causing the sheet to bend. Another stress reversal may occur in the sheet after it has passed the draw radius, depending on the magnitude of the draw radius and the clearance between punch and die [2]. Examples for springback of hat profiles are shown in later sections.

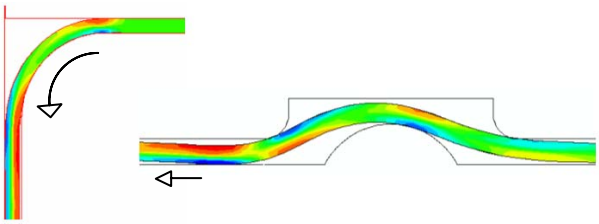

**Figure 2.** Stresses in a sheet passing a draw radius (left) and a draw bead (right).

Cyclic plastic deformation may also occur when a sheet passes a draw bead (Figure 2, right). Although the parts of the sheet which have passed a draw bead will usually later be removed, the force exerted by the draw bead may affect the stresses in the whole part [2].

From the foregoing it is clear that springback is directly related to the residual stresses remaining in the material after one or more reversals of plastic deformation. Hence it is essential to use constitutive material models which are capable of describing all relevant aspects of the material behaviour under such conditions.

Probably the most important aspect is the Bauschinger effect, which means that after a load reversal the flow stress can be significantly smaller than before. The Bauschinger effect is taken into account by the Chaboche model [3][4], which discern between isotropic and kinematic hardening. These models are used in this work,

and they include also the rate dependency of the flow stress.

A less obvious aspect is the fact that the modulus of elasticity appears to be smaller during unloading from the plastic state than during the first loading, and to decrease further during subsequent reloadings and unloadings. This has been observed repeatedly in the literature [5][6][7][8][9], and also by the present authors. Although this phenomenon is probably a consequence of microplasticity, it is described most efficiently in the simulations as a reduction of the elastic modulus. Its influence on the springback may be substantial.

One of the most important factors in sheet forming is the plastic anisotropy resulting from the crystallographic texture evolving during rolling. The classical phenomenological models for plastic anisotropy [10][11] are extended to include the Bauschinger effect. They are compared with more general phenomenological formulations which allow rotations and distortions of the yield surface during deformation [12]. Finally the phenomenological models are compared with results of the visco-plastic self-consistent (VPSC) texture model [13][14]. Models with evolving anisotropy [12][13][14] allow to answer the question whether it is necessary to update the anisotropy during a forming operation or whether it suffices to do the calculation with the initial anisotropy resulting from the rolling texture. In [15] a plastic strain of 20% is mentioned below which no update is necessary.

Compared to the plastic anisotropy, the anisotropy of the elastic properties [16][17] plays a smaller role, but it cannot always be neglected, if a high accuracy is required.

## Tension-compression tests

To determine the parameters of the plasticity models it is necessary to perform tension-compression tests with considerable strain. For this purpose a special test rig with a stiff loading frame and a new specimen design were developed (Figure 3) in order to avoid buckling of the sheet specimens during compression.

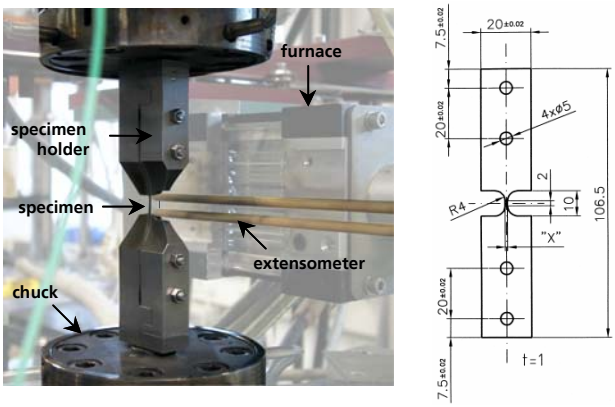


**Figure 3.** Test rig and specimen design for the determination of cyclic stress-strain curves.

With this experimental method several types of mild and high strength steels as well as magnesium, aluminium and copper alloys were tested successfully. The stiffness of the rig allows tension-compression tests up to 20% strain. Figure 4 shows a result for the high strength steel DP-K 34/60+Z tested at room temperature at a nominal strain rate of $4 \cdot 10^{-4}$ $s^{-1}$.

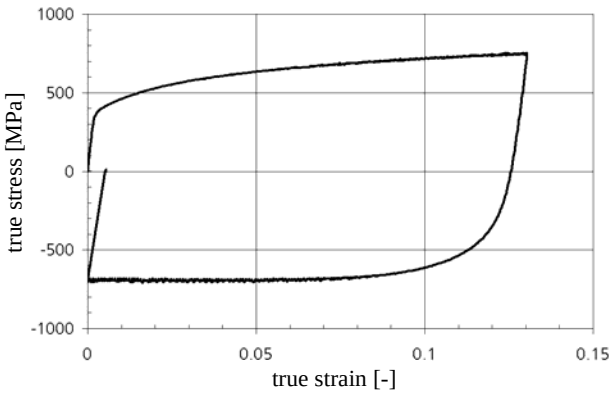


**Figure 4.** Tension-compression response of the high strength steel DP-K 34/60+Z.

Apparently the material starts to yield in compression at a far smaller amount of stress than the stress at the reversal point. This is an aspect of the Bauschinger effect, and it is described correctly by the models used in this work (see Figure 8). Further the reduction of the tangent modulus from the first loading over the unloading from the tensile state to the final unloading is obvious.

## The Chaboche model and its modifications

*The model equations*

To describe the Bauschinger effect we use a material model based on the well-known formulation of Chaboche [3][4] for nonlinear isotropic-kinematic hardening which is modified with respect to forming simulation.

The yield function is defined as:

$$f = \sigma_{eq} - R - \sigma_0 \tag{1}$$

with the material parameter $\sigma_0$ and the equivalent stress

$$\sigma_{eq} = \sqrt{\frac{3}{2} S_{ij}^{ef} S_{ij}^{ef}} \tag{2}$$

where $S_{ij}^{ef}$ is an effective deviatoric stress

$$S_{ij}^{ef} = S_{ij} - \alpha_{ij} \tag{3}$$

$$S_{ij} = \sigma_{ij} - \frac{1}{3}\sigma_{kk}\delta_{ij} \tag{4}$$

The hardening variables $R$ and $\alpha_{ij}$ describe isotropic and kinematic hardening, respectively; $\alpha_{ij}$ is called backstress. Plastic flow obeys the normality rule

$$\dot{\varepsilon}_{ij}^{vp} = \dot{p}\frac{3}{2}\frac{S_{ij}^{ef}}{\sigma_{eq}} \tag{5}$$

For the rate independent case the equivalent plastic strain rate $\dot{p}$ can be calculated from the consistency condition

$$\dot{f} = 0 \tag{6}$$

whereas for the rate dependent case it is given by

$$\dot{p} = \left\langle \frac{\sigma_{eq} - R - \sigma_0}{K} \right\rangle^n \tag{7}$$

$n$ and $K$ are constants; $\langle x \rangle = x$ if $x > 0$ and $\langle x \rangle = 0$ if $x < 0$. The hardening variables obey the evolution equations

$$\dot{R} = b(Q - R)\dot{p} \tag{8}$$

$$\dot{\alpha}_{ij} = c(\frac{2}{3} r \dot{\varepsilon}_{ij}^{vp} - \alpha_{ij})\dot{p} \tag{9}$$

where $b$, $Q$, $c$ and $r$ are material parameters. The use of more than one back-stress increases the flexibility of the model in describing stress-strain curves [18].

$$\alpha_{ij} = \sum_{m=1}^{M} \alpha_{ij}^{(m)} \tag{10}$$

$$\dot{\alpha}_{ij}^{(m)} = c^{(m)}(\frac{2}{3} r^{(m)} \dot{\varepsilon}_{ij}^{vp} - \alpha_{ij}^{(m)})\dot{p} \tag{11}$$

An advantage of the above formulation is that it is directly integrable for the uniaxial case and fitting of the model to experimental data occurs just by fitting of the equation

$$\sigma = N(Q(1 - e^{-bp}) + \sigma_0) + KN\dot{p}^{1/n} + \sum_{m=1}^{M} [Nr^{(m)} + (\alpha_{p_0}^{(m)} - Nr^{(m)})e^{-c^{(m)}(p - p_0)}] \tag{12}$$

applied for any half-cycle of the stress-strain curve. Here $N = \text{sign}(\sigma - \alpha)$ is positive for tension and negative for compression, $p_0$ and $\alpha_{p_0}^{(m)}$ are the values of $p$ and $\alpha^{(m)}$, respectively, at the last change of the plastic strain rate.

*Application to the draw bending test*

To assess an influence of the hardening model on the predicted springback a draw bending test for steel H220 is modelled. The material parameters are for the isotropic case $\sigma_0$ = 200 MPa, $Q$ = 265.1 MPa, $b$ = 8.4, $r$ = 0, $c$ = 0 and for the kinematic case $\sigma_0$ = 200 MPa, $Q$ = 0, $b$ = 0, $r$ = 265.1 MPa, $c$ = 8.4. The sheet thickness and draw radius were 1.5 mm and 8 mm, respectively. All simulations in this chapter were performed with the FE code ABAQUS using five volume elements over the sheet thickness. Figure 5 shows the distribution of the stress component in drawing direction over the sheet thickness for material that has passed the draw radius.

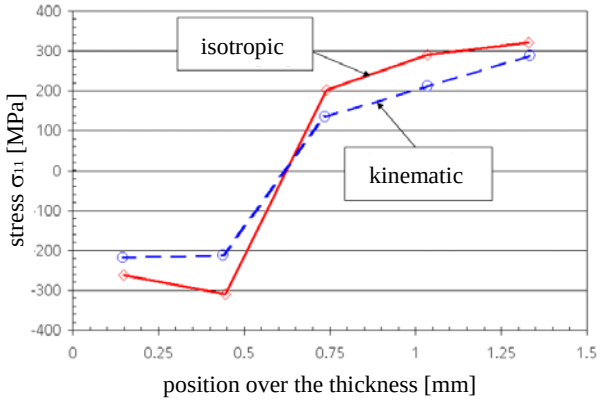


**Figure 5.** Stress distribution over the sheet thickness at the end of drawing depending on the type of hardening.

The calculation with isotropic hardening gives stresses up to 100 MPa higher than with kinematic hardening. Figure 6 shows the shape of the hat profile after springback predicted with both models. (Here and in the sequel only one half is shown because of symmetry). The difference between isotropic and kinematic hardening is moderate here, but it becomes larger for 1 mm draw radius, where even the direction of springback is different for the two models [2].

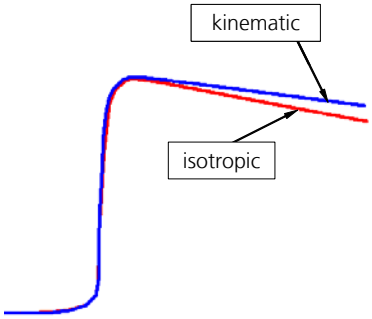


**Figure 6.** Springback predicted with different hardening models.

Figure 7 shows that the reaction force of a drawing bead is about 20% higher for isotropic hardening than for kinematic hardening.

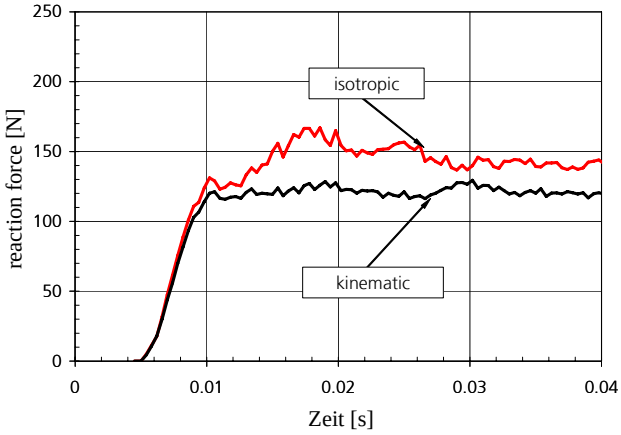

**Figure 7.** Reaction force of a draw bead calculated with different hardening models.

*Apparent reduction of the modulus of elasticity*
As mentioned in the introduction the slope of the stress-strain curves after reversals of the straining direction decreases with increasing number of reversals. Although this is probably the result of microplastic processes, it is described most efficiently by a decreasing modulus of elasticity. On the basis of experimental observations an exponential dependence of the elastic modulus on the cumulative equivalent plastic strain $p$ was suggested [2]

$$E = E_0 - A(1 - e^{-sp}) \tag{13}$$

where $E_0$ is the initial value of the elastic modulus and $A$ and $s$ are empirical constants.

*Application to a dual phase steel and a cross girder*
Figure 4 shows that the measured tension-compression curve of a dual phase steel can be described accurately if a variable elastic modulus and two back-stresses are used with the parameter set $\sigma_0$ = 309.7 MPa, $Q$ = 131.2 MPa, $b$ = 20.1, $r_1$ = 140 MPa, $c_1$ = 39.8, $r_2$ = 150.1 MPa, $c_2$ = 249.9, $E_0$ = 200 GPa, $A$ = 70 GPa and $s$ = 10.

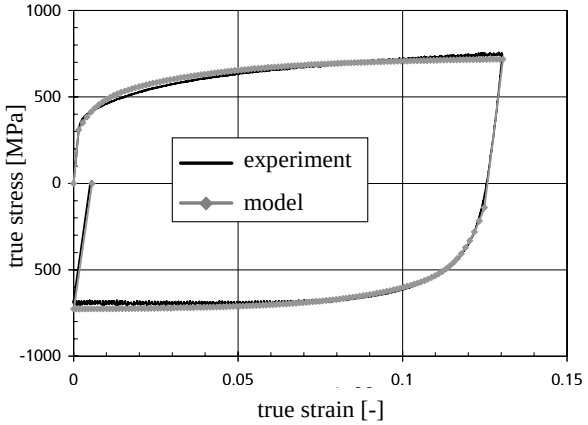


**Figure 8.** Tension-compression test and its description by the extended Chaboche model (steel DP-K 34/60+Z).

The validity of this model was demonstrated in cooperation with ThyssenKrupp Stahl AG for the cross girder shown in Figure 9, which is made from the same dual phase steel. As the figure shows, the measured springback is predicted with only moderate accuracy by the classical Chaboche model, but very accurately by the extended model.

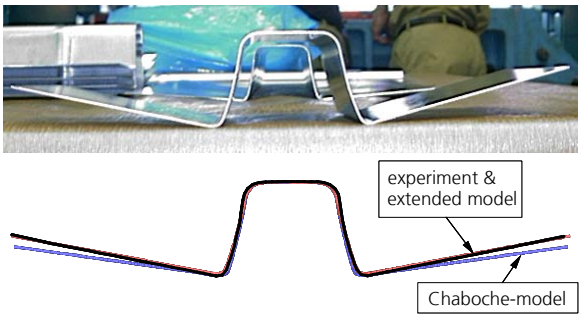


**Figure 9.** Predicted and measured springback of a cross girder.

*Influence of the strain-rate dependency*
Strain rates may locally be high during forming processes, especially at small draw radii [2]. Figure 10 shows the history of the strain rates in each of the five elements over the sheet thickness during the draw bending test. The velocity of the punch was increased continuously to the maximum value of 0.06 m/s. The sheet thickness is 1.5 mm and draw radius is 1 mm. The strain rates near the sheet surface have values up to nearly 40 $s^{-1}$.

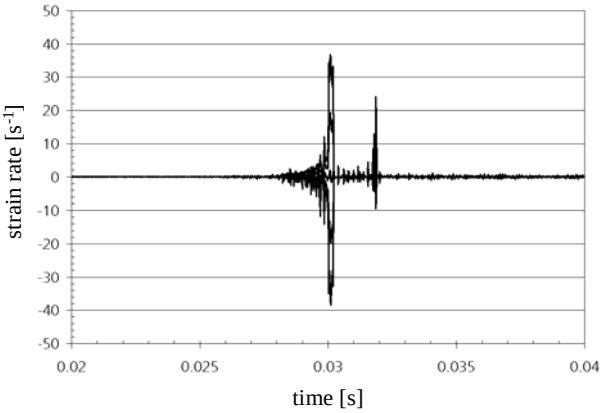


**Figure 10.** Strain rates in the elements across the sheet thickness during the pass over the draw radius.

For the dual phase steel DP-K 34/60+Z the strain-rate dependency is known from [19]: $n$ = 4.8, $K$ = 60. This means that the stress level at the strain rate 40 $s^{-1}$ is about 130 MPa higher than in static case. Figure 11 shows the influence of the strain rate dependency on the predicted springback.

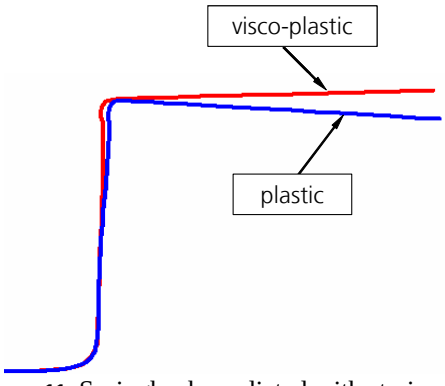


**Figure 11.** Springback predicted with strain-rate dependent and strain-rate independent models.

### Elastic and plastic anisotropy and its evolution

As has already been mentioned, a strong orthotropic anisotropy of the elastic and plastic properties can develop in the sheet during a rolling process. Thus the elastic properties are characterized by an orthotropic tensor with nine independent coefficients [2]. Figure 12 shows the variation of Young's modulus as a funtion of the angle between the tensile axis and the rolling direction calculated by the VPSC model for a cold rolled copper sheet after 80% thickness reduction. In this case Young's modulus varies by 10%.

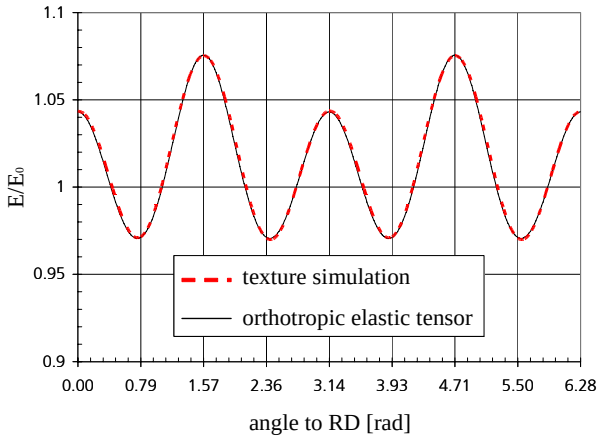


**Figure 12.** Anisotropy of Young's modulus.

Here $E_0$ means the isotropic value of the elastic modulus before rolling. Experimental results for steel can be found in [17]. The influence of the elastic anisotropy on the springback was shown to be negligible, except possibly for parts with very high geometrical requirements [2].

Plastic anisotropy in metal sheets has traditionally been described by anisotropic yield surfaces, e.g. according to Hill [10] or to Barlat [11]:

$$f^{Hill} = S_{ij} M_{ijkl} S_{kl} - \sigma_0^2 \tag{14}$$

$$f^{Barlat} = a\left|K_1 + K_2\right|^m + a\left|K_1 - K_2\right|^m + (1-a)\left|2K_2\right|^m - \sigma_0^2 \tag{15}$$

with

$$K_1 = \frac{\sigma_{11} + h\sigma_{22}}{2}, \qquad K_2 = \sqrt{\left(\frac{\sigma_{11} - h\sigma_{22}}{2}\right)^2 + p^2\sigma_{12}^2} \tag{16}$$

where the components of the forth order tensor $M_{ijkl}$ and the constants $a$, $h$ and $p$ are anisotropy parameters which can be determined from the $r$-values [10][11]. The exponent $m$ depends on the lattice of the material. For fcc metals $m = 8$ and for bcc-metals $m = 6$ leads to good agreement with the results of texture simulations [20].

To incorporate the Hill'48 criterion in the Chaboche model one replaces the equivalent stress in (1) by

$$\sigma_{eq} = \sqrt{S_{ij}^{ef} M_{ijkl} S_{kl}^{ef}} \tag{17}$$

and the equation for the visco-plastic strain rate (5) by

$$\dot{\varepsilon}_{ij}^{vp} = \dot{p}\frac{M_{ijkl} S_{kl}^{ef}}{\sigma_{eq}} \tag{18}$$

Additionally, to ensure an equivalent evolution of the hardening variables $R$ and $\alpha_{ij}$ for purely isotropic and purely kinematic hardening during uniaxial proportional loading the plastic potential must be modified and the evolution equation for the back-stress must be replaced by:

$$\dot{\alpha}_{ij} = c\left(r\frac{S_{ij}^{ef}}{\sigma_{eq}} - \alpha_{ij}\right)\dot{p} \tag{19}$$

The same procedure can be applied for the Barlat criterion [2].

Differences between the yield functions can be significant. As an example Figure 13 shows the yield criteria of von Mises, Hill'48 and Barlat for the aluminium alloy Al 2090-T3 ($r_0 = 0.21$, $r_{90} = 0.69$) [21]. For the Barlat criterion $m = 8$ was used. All yield surfaces have a common point for uniaxial tension in 1 direction. The difference between the Hill and the Barlat criterion are particularly significant near plane-strain conditions ($\sigma_{22} = 2\sigma_{11}$), which frequently prevail during deep drawing.

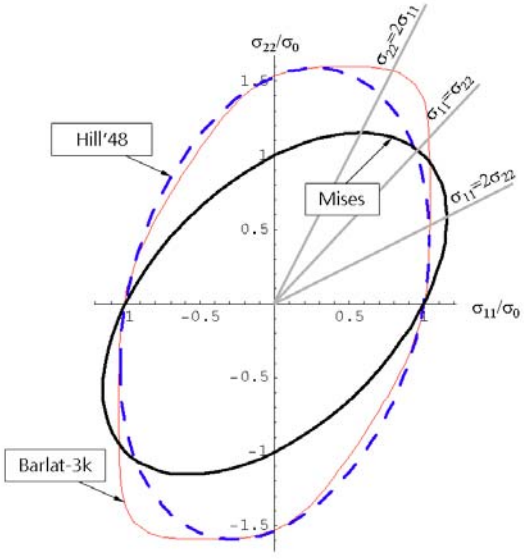


**Figure 13.** Anisotropic yield surfaces for the aluminium alloy Al 2090-T3 described by different yield functions.

Because of the different shapes of the Hill'48 and the Barlat yield surfaces, they can lead to significantly different predictions even for isotropic material. This is illustrated by the following simulation of the draw bend-

ing test with draw radius 5 mm for isotropic material ($r_0 = r_{90} = r_{45} = 1$). The Chaboche model with isotropic hardening was used in conjunction with the Hill or the Barlat criterion. The material parameters were fitted to data from [21]: $\sigma_0 = 279.6$ MPa, $Q = 271.0$ MPa and $b = 5.9$.

Figure 14 shows the stresses in the sheet when it passes through the draw radius. Apparently the Hill criterion gives higher stresses than the Barlat criterion during the forming stage and unloading. Consequently the springback is also greater.

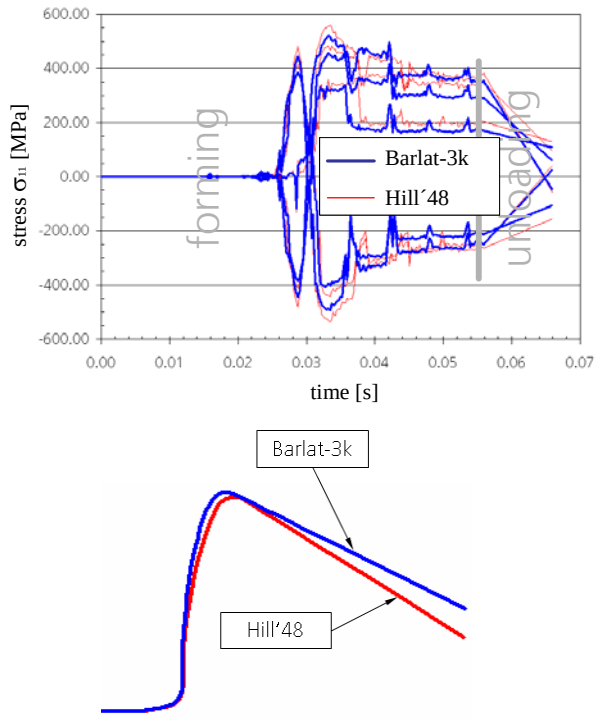


**Figure 14.** Stresses at different locations over the sheet thickness during forming and unloading and the resulting shape of the hat profile after springback.

Because of the sensitive reaction of the simulated springback to the shape of the yield surface more attention should be paid to its accurate description including the evolution during plastic deformation. Different strategies were proposed to describe the evolution of the anisotropic yield surface phenomenologically. One of them is to represent the yield function in polynomial form with hardening tensors of growing complexity [12]:

$$f = V^{(0)} + V_{ij}^{(1)} S_{ij} + S_{ij} V_{ijkl}^{(2)} S_{kl} + \\ + S_{ij} S_{kl} V_{ijklmn}^{(3)} S_{mn} + \ldots \qquad (20)$$

where the hardening tensors $\mathbf{V^{(i)}}$ are internal variables. In this framework the Chaboche model corresponds to the isotropic second order tensor

$$V_{ijkl}^{(2)} = \frac{3}{2} I_{ijkl} \qquad (21)$$

with identity tensor $I_{ijkl}$.

To allow a shape change of the yield surface in stress space one can extend the Chaboche model according to

$$f = \frac{3}{2}\left[S_{ij}^{ef} \beta_{ijkl} S_{kl}^{ef} + S_{ij}^{ef} S_{kl}^{ef} \gamma_{ijklmn} S_{mn}^{ef}\right] + (\sigma_0 + R)^2 \qquad (22)$$

where $\beta_{ijkl}$ and $\gamma_{ijklmn}$ are the anisotropic tensors which are responsible for the rotation and the shape change of the yield surface. The main difference in comparison with the yield functions describing a stationary anisotropy is that the anisotropic tensors in this case obey evolution equations, which have the form

$$\dot{\beta}_{ijkl} = c_\beta \left(b_\beta \frac{\partial f}{\partial \beta_{ijkl}} - \beta_{ijkl}\right)\dot{p} \qquad (23)$$

$$\dot{\gamma}_{ijklmn} = c_\gamma \left(b_\gamma \frac{\partial f}{\partial \gamma_{ijklmn}} - \gamma_{ijklmn}\right)\dot{p} \qquad (24)$$

with the empirical parameters $c_\beta$, $b_\beta$, $c_\gamma$ and $b_\gamma$. Models with changing shapes of the yield surface are called distortional hardening models.

Next the phenomenological models are compared with results of the VPSC texture model. Figure 15 shows calculated yield surfaces for pure aluminium after different deformation histories. Figure 15a represents the yield surface directly after rolling with 60% height reduction. For this case the Chaboche model combined with the Hill criterion is adjusted to the yield surface calculated with the VPSC model. Figures 15b and 15c were calculated for the case that the rolled material is strained in uniaxial tension by 50% in rolling direction (Fig. 15b) and transverse direction (Fig. 15c). The data points represent the results of the VPSC model, the curves denoted by Chaboche and Hill are calculated with a constant anisotropy tensor $\beta_{ijkl}$, while the curves denoted by distortional hardening are adjusted to the texture model by an evolving $\beta_{ijkl}$. In this case it is not necessary to use the sixth order tensor $\gamma_{ijklmn}$, since the shape of the yield surface remains nearly elliptic, which can be described by an evolving $\beta_{ijkl}$ including the rotation of the axes of the ellipse.

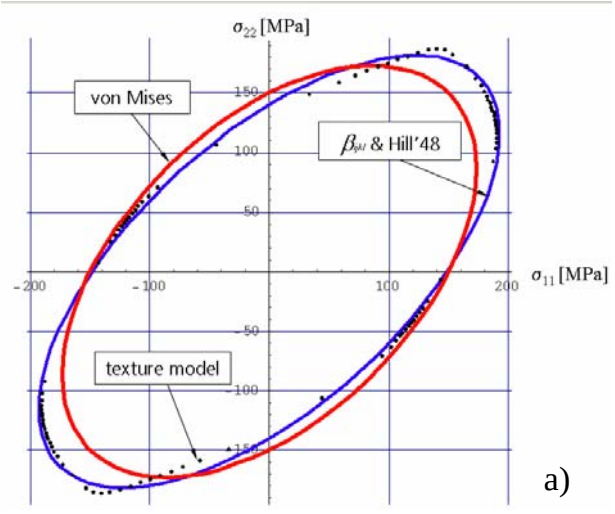


a)

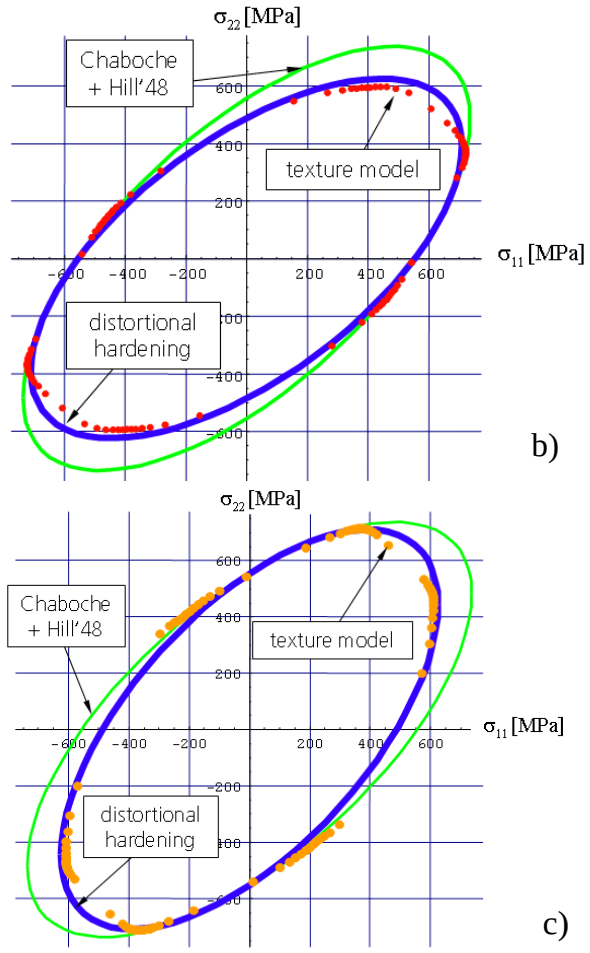


**Figure 15.** Yield surfaces predicted with the VPSC texture model compared to phenomenological models with and without evolving anisotropy.

## Conclusions

A novel experimental-numerical approach based on tension-compression tests, phenomenological material models and texture simulations was presented. It was shown that predictions of springback in forming simulations can be improved by using advanced material models. Usually the most important factors to be considered are the Bauschinger effect, the apparent decrease of Young's modulus with the number of strain reversals, the anisotropy and sometimes its evolution during the forming process, and strain rate effects. Texture modelling can be used to predict elastic and plastic anisotropy and to calibrate phenomenological models for evolving anisotropy. The parameters of models including isotropic and kinematic hardening can be determined from a newly developed tension-compression tests.

## References

[1] D.Y. Yang, S.I. Oh, H. Huh, Y.H. Kim: NUMISHEET 2002: Proceedings of 5th international conference and workshop on numerical simulation of 3D sheet forming processes, Jeju Island, Korea, Vol.1 (2002)
[2] A. Krasovskyy: Verbesserte Vorhersage der Rückfederung bei der Blechumformung durch weiterentwickelte Werkstoffmodelle. Thesis Fakultät für Maschinenbau der Universität Karlsruhe, Germany (2005)
[3] J.L. Chaboche, K. Dang-Wan, G. Cordier: Modelization of the strain memory effect on the cyclic hardening of 316 stainless steels. SMiRT-5, Div. L, Paper No. L. 11/3 (1979)
[4] J. Lemaitre, J.L. Chaboche: Mechanics of solid materials. Cambridge University Press (1990)
[5] R.M. Cleveland, A.K. Ghosh: Inelastic effects on springback in metals. Int. J. Plasticity 18 (2002) 769-785
[6] E. Doege, H. Zenner, H. Palkowski, A. Hatscher, R. Schmidt-Jürgensen, S. Kulp, C. Sunderkötter: Einfluss elastischer Kennwerte auf die Eigenschaften von Blechformteilen. Mat.-wiss. u. Werkstofftech. 33 (2002) 667-672
[7] S. Thibaud, J.C. Gelin: Influence of initial and induced hardening on the formability in sheet metal forming. IJFP Material Processing Defects 5 (2002) 505-520
[8] F. Yoshida, T. Uemori: A model of large-strain cyclic plasticity describing the Bauschinger effect and workhardening stagnation. Int. J. Plasticity 18 (2002) 661-686
[9] F. Yoshida, T. Uemori, K. Fujiwara: Elastic-plastic behavior of steel sheets under in-plane cyclic tension-compression at large strain. Int. J. Plasticity 18 (2002) 633-659
[10] R. Hill: A theory of the yielding and plastic flow of anisotropic metals. Proc. Roy. Soc. A193 (1948) 281-297
[11] F. Barlat, J. Lian: Plastic behavior and stretchability of sheet metals. Part I: A yield function for orthotropic sheets under plane stress conditions. Int. J. Plasticity 5 (1989) 51-66
[12] U. Kowalsky, H. Ahrens, D. Dinkler: Distorted yield surfaces-modeling by higher order anisotropic hardening tensors. Comp. Mater. Sci. 16 (1999) 81-88
[13] U.F. Kocks, C.N. Tome, H.-R. Wenk: Preferred orientations in polycrystals and their effect on Materials properties. Texture and Anisotropy. Cambridge University Press (1998)
[14] T. Walde: Modellierung der Textur- und Anisotropieentwicklung beim Walzen – Kopplung der Finite Elemente Methode mit mikrostrukturbasierten Modellen. Thesis Fakultät für Maschinenbau der Universität Karlsruhe, Germany (2004)
[15] K. Kowalczyk, W. Gambin: Model of plastic anisotropy evolution with texture-dependent yield surface. Int. J. Plasticity 20 (2003) 19-54
[16] A. Bertram, T. Böhlke: Simulation of texture induced elastic anisotropy of polycrystalline copper, Comp. Mater. Sci. 16 (1999) 2-9
[17] T. Lauwagie, H. Sol, G. Roebben, W. Heylen, Y. Shi, O. Van der Biest: Mixed numerical-experimental identification of elastic properties of orthotropic metal plates. NTDT&E Int. 36 (2003) 487-495
[18] J.L. Chaboche, G. Rousselier: On the plastic and viscoplastic constitutive equations – Part 1: Rules developed with internal variable concept. J. Press. Vessel Technol. 105 (1983) 153-158
[19] L. Kessler, Th. Gerber: Characterisation and behaviour of steel sheet materials for linking FEM-Simulation in successive stamping and crash processes. In: Proc. EUROPAM 2001, Heidelberg, Germany (2001)
[20] R.W. Logan, W.F. Hosford: Upper-bound anisotropic yield locus calculations assuming <111> pencil glide. Int. J. Mech. Sci. 22 (1980) 419-430
[21] J.W. Yoon, F. Barlat, F. Pourboghrat, K. Chung, D.Y. Yang: Earing predictions based on asymmetric nonquadratic yield function. Int. J. of Plasticity 16 (2000) 1075-1104